Temperature and Velocity Profiles in Sooting Free Convection Diffusion Flames

James A. Ang,* Patrick J. Pagni,† and Thomas G. Mataga*
University of California, Berkeley, California
and
Janice M. Margle‡ and Valerie J. Lyons§
NASA Lewis Research Center, Cleveland, Ohio

Temperature and velocity profiles are measured for cyclohexane, n-heptane, ethyl alcohol and isooctane free, laminar, boundary-layer, sooting, diffusion flames. Temperatures are measured with 3 mil Pt/Pt-13%Rh thermocouples. Corrected gas temperatures are derived by performing an energy balance of convection to and radiation from the thermocouple bead incorporating the variation of air conductivity and platinum emissivity with temperature. Other effects are shown to be negligible. Velocities are measured using laser Doppler Velocimetry techniques. Profiles are compared with previously reported analytic temperature and velocity fields. Comparison of theoretical and experimental temperature profiles suggests improvement is needed in the analytical treatment that accounts for the effects of thermal cracking of the fuel. The velocity profiles are in good agreement, with the departure of theory from observation partially due to the small fluctuations inherent in these free flows.

Introduction

TEMPERATURE and velocity profiles across free-flow boundary-layer diffusion flames are obtained experimentally. These measurements compliment previously reported soot volume fraction measurements[1] and analytic determination of temperature and velocity profiles including approximate radiation effects.[2,3] The basic flowfields in this configuration are well documented in the literature,[4-6] providing a norm from which the effects of soot in the combustion field can be discerned. The flame radiative heat-transfer increase due to soot in the combustion field may be undesirable (e.g., in an engine combustion chamber or a compartment fire) or desirable (e.g., in a furnace). By developing a model for the formation of soot particles, radiative heat transfer in combustion processes can be more accurately determined. Experimental soot volume fraction profiles are available to permit modeling of the soot formation rates. However, accurate temperature and velocity fields are necessary before a model for soot formation can be developed. Soot particle trajectories can be found given velocity profiles within the boundary layer. It has been previously shown that soot temperatures are locked to the gas temperature.[3] Therefore, these trajectories plus a knowledge of the temperature field can be used to estimate the temperature dependent evolution of the soot particle size distribution. Recently Santoro et al.[7] presented measurements in a buoyant coannular laminar diffusion flame of temperature, velocity, and soot volume fraction data in a similar study on soot formation. Many related studies of the forced flow laminar boundary-layer diffusion flame have been made,[8-11] but there have been few experimental studies of the free-flow, laminar boundary-layer diffusion flame.

Presented as Paper 86-0575 at the AIAA 24th Aerospace Sciences Meeting, Reno, NV, Jan. 6-9,1986; received Nov. 12, 1986; revision received Jan. 16, 1987.

*Research Assistant, Department of Mechanical Engineering.
†Professor, Department of Mechanical Engineering.
‡Visiting Scientist, (presently with Pennsylvania State University, Abington, PA).
§Research Scientist.

This paper presents experimentally determined temperature and velocity fields in a free-flow, vertical, boundary-layer diffusion flame. Temperatures are obtained using 3 mil Pt/Pt-13%Rh fine-wire thermocouples. The radiation correction to determine gas temperatures from the thermocouple output includes the influence of soot and of the temperature dependence of physical properties. Comparisons with analytical temperature profiles reveal possible areas for improvement of the modeling of diffusion flames. Streamwise velocities, measured using laser Doppler velocimetry, are in reasonable agreement with predictions.

Temperature Fields

These measurements are made in flames supported by evaporating n-heptane, cyclohexane, isooctane, and ethyl alcohol liquid fuels. The combustion apparatus is a 15 wide × 8 high × 2.5 cm block of Fiberfrax ceramic fiber material, saturated with fuel and flush mounted on a Marinite vertical wall. Figure 1 is a schematic diagram of this combusting boundary layer. Temperature and velocity profiles are measured at 2 and 4 cm downstream from the leading edge of the fuel wick surface. Low-frequency flame oscillations prohibited measurements beyond 6 cm downstream. Measurements in the transverse direction are taken in half-millimeter increments with 0.1 mm accuracy. All measurements are made at atmospheric pressure in air.

Temperatures are measured with a 3 mil (0.08 mm) Pt/Pt-13%Rh thermocouple mounted on a micrometer stage. Figure 2 is a scanning electron microspcope photograph of a bead with an approximately 7 mil (0.17 mm) diameter. This photograph also reveals remnants of soot especially in the space between the leads, where soot can be expected to accumulate in the stagnant region downstream of the bead. The thermocouple bead is suspended horizontally with its 1 cm leads parallel to the fuel surface along an isotherm to minimize conduction losses from the leads. The millivolt potentials are converted to temperatures using the polynomial fits given by Quinn.[12] These functions accurately reproduce the tables and are better suited to numerical calculation. Three zones requiring different temperature measurement proceedures exist: 1) between the wall and soot layer and beyond the flame zone, 2) within the soot layer, and 3) within the flame zone. Zone 1 consists of the clear regions in Fig. 1. There the temperature measurements are straightforward. One begins at the wall and

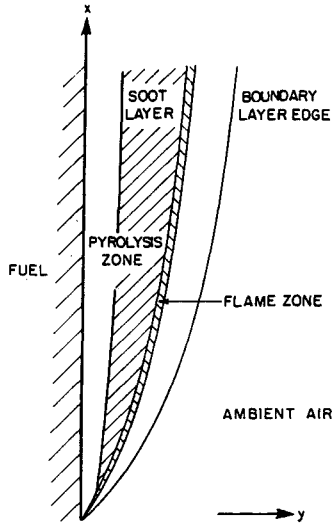

Fig. 1 Schematic diagram of a steady, buoyancy-driven, two-dimensional, laminar, radiating, combusting, boundary-layer flame with soot on a vertical pyrolyzing fuel slab.

moves outward at fixed increments or begins at ambient conditions a known distance from the wall and moves inward. The thermocouple is positioned using a micromanipulator with 0.05 mm resolution.

The difficulties of making temperature measurements in a soot layer, zone 2—the left slanted hatched region of Fig. 1, are well known.[13,14] The presence of soot on the thermocouple bead will reduce the bead temperature by several hundred degrees. This drop is primarily due to the soot emissivity (0.8) exceeding the platinum emissivity (0.2) by a factor of four. The increase in size due to soot deposition driven by thermophoresis[15] plays a secondary role in reducing the temperature.[14] Temperature measurements in the soot zone are taken by rapidly moving a clean thermocouple from the flame zone into the desired position and carefully extrapolating the temperature back to a time before soot accumulation.[13] Moving the bead to the flame layer between readings burns off the soot coating. In this procedure, thermophoresis serves to shield the bead from soot particles because the bead has a finite response time, here ~ 0.03 s, and the bead is being moved from the hot flame zone to the cooler sooty region at ~ 1 cm/s; so, initially the bead will be at an elevated temperature with respect to the surrounding soot laden gas. Soot can begin to accumulate only after the bead temperture has dropped below the local gas temperature. Starting at the flame temperature, temperature drops linearly with time as the nearly linear temperature field is traversed at a constant velocity. A time mark is tripped when the thermocouple reaches the desired location identifying T (0). In addition, a more slowly varying temperature drop $T(t)$ is recorded as soot accumulates on the bead. This history is curve fit and extrapolated back to the time marker to verify T (0), which is taken as the bead temperature for use in Eq. (7) below at that location.

Often silicon dioxide (SiO_2) or yttrium oxide (Y_2O_3) coatings are used to prevent exothermic reactions on the possibly catalytic platinum surface. Such reactions can lead to erroneously high temperatures. The use of these coatings in our experiment was discouraged by several factors. SiO_2 coatings in a reducing atmosphere can lead to the formation of a silicon solid solution in the Pt and Pt-13%Rh legs of the thermocouple. This would shift the Fermi energy levels of the two components of the junction and decalibrate the potential difference output.[16] In addition, above 1800 K the SiO_2 melts and flows into beads. As a practical constraint, yttrium oxide coatings are avoided for their toxic nature. An additional consideration is that most catalytic reactions involve radical

Fig. 2 Electron micrograph (180×) of the Pt/Pt-13%Rh thermocouple bead. Wire and bead diameters are 0.08 mm and 0.17 mm, respectively. The dark patches are remnants of soot.

recombination.[17] This makes coating of platinum thermocouples important for premixed flames, but much less important in diffusion flame thermometry. With diffusion flames, radicals exist only in the very narrow flame layer, where gas phase reactions are very rapid.[18] Also, the addition of a SiO_2 or Y_2O_3 layer would increase the radiation correction and significantly complicate the energy balance on the bead.

An energy balance between convection to and net radiation away from the spherical bead is required to extract the true gas temperature from the thermocouple bead temperature. By aligning the leads along an isotherm, it is assumed that there is no conduction down the leads. The convective heat-transfer coefficient is approximated using Nusselt number correlations and including the variation in the thermal conductivity of air with temperature. In order to properly characterize the radiation loss, a platinum emissivity as a function of temperature is also used. Radiation transfer from the surroundings to the bead are included, although for this flame the only significant radiation flux is from the bead. Note that for enclosure fires the external radiation flux may be important. The Reynolds number for a sphere the size of the thermocouple bead is less than 1, even at the maximum buoyant velocity of 1 m/s. For a sphere in this flow regime the Nusselt number[19] is

$$Nu = hD/k = 2 + 0.37Re^{0.6}Pr^{0.33} \tag{1}$$

for all Reynolds Re and Prandtl Pr numbers of interest. Here, h is the average heat transfer coefficient, D the bead diameter, and k the gas thermal conductivity. This provides an average heat-transfer coefficient for the bead as good as the spherical assumption. The thermocouple leads do not alter this heat-transfer coefficient, while they do reduce the "wetted" area of the bead. Since for the cylindrical leads, $Nu \sim 1$ and $D_{\text{leads}} \sim D/2$, h is similar for the leads and bead. This uniformity of h yields $T_{\text{leads}} = T_b$ and justifies neglecting conduction. The thermophysical properties of air are assumed to approximate the gas surrounding the bead. In order to improve the

accuracy of the heat-transfer coefficient, the conductivity of air is curve fit by a third-order polynomial,

$$k = C_0 + C_1\theta + C_2\theta^2 + C_3\theta^3, 300 < T_{\text{gas}} < 2200\,\text{K} \qquad (2)$$

where $\theta = T_{\text{gas}}/2200$ K with $C_0 = 0.00370$, $C_1 = 0.191$, $C_2 = -0.174$, and $C_3 = 0.139$, and the units are w/m·K. The treatment of radiation in this energy balance is simplified by using the optically thin approximation, i.e., the soot emits but it does not attenuate radiation. Radiation exchange between the bead, wick surface, soot, and ambient atmosphere are allowed. In practice, the dominant radiative transfer is from only the bead. But for solid and sooty fuels, or in enclosures, the other radiative sources can be important. Surfaces are assumed to be in local thermal equilibrium, diffuse, and gray, except for the wall and ambience, which are assumed black. The net radiation flux out of the bead is

$$q_r = \epsilon_b\sigma T_b^4 - \alpha_b F_{bw}\sigma T_w^4 - \alpha_b F_{b\infty}\sigma T_\infty^4 - \alpha_b F_{bs}\epsilon_s\sigma T_s^4 \qquad (3)$$

where the subscripts indicate bead b, soot s, fuel wick w, and ambient ∞; ϵ is the emissivity, α the absorptivity, and F_{ij} the view factor, here all equal to 0.5, since half the bead sees the wall and half sees the ambience. An average soot emissivity for the whole soot layer is determined using the assumption of a uniform soot absorption coefficient.[2] The soot zone then becomes a plane surface at T_s with ϵ_s so that the view factor from the bead to the soot is also 0.5. Kirchoff's law and the gray assumption are applied to substitute the emissivity for the absorptivity of the platinum bead. The net radiation flux out of the bead reduces to

$$q_r = 0.5\epsilon_b\sigma[2T_b^4 - T_w^4 - T_\infty^4 - \epsilon_s T_s^4] \qquad (4)$$

The emissivity of the bead can be found as a function of its temperature. In an analysis outlined by Jakob,[19] Maxwell's wave equations can be solved to yield the complex indices of refraction for a metal as a function of its electrical resistivity. In the limit of low resistivity and assuming a large index of refraction, which is true for metals, Jakob gives the hemispherical total emissivity as

$$\epsilon = 0.751(r_e T)^{1/2} - 0.396 r_e T,\ 0 < r_e T < 0.2 \qquad (5)$$

where, for platinum, $r_e \approx r_{e,273}T/273$, with T in degrees K and $r_{e,273} = 11\times10^{-6}\Omega\cdot\text{cm}$.[20] Note that the emissivity is nearly linear with T and $q_r \sim T^5$, since Eq. (4) becomes

$$\epsilon = 1.507\times10^{-4}T_b - 1.596\times10^{-8}T_b^2,\ 0 < T < 2230\,\text{K} \qquad (6)$$

This equation is confirmed by the comparison with experimental data from the Honeywell Research Center[21] shown in Fig. 3. Note that for temperatures where radiation is important, predicted and observed emissivities agree to within 1%.

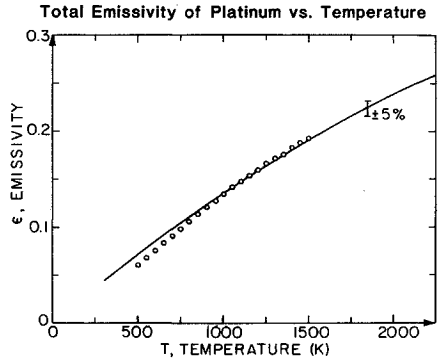

Fig. 3 Total emissivity of platinum vs temperature based on Jakob's theoretical calculation and experimental data from the Honeywell Research Center.

The gas temperature is then found from $\dot{q}_c'' = h\Delta T = \dot{q}_r''$,

$$T_g = T_b + 0.5\epsilon_b\sigma[2T_b^4 - T_w^4 - T_\infty^4 - \epsilon_s T_s^4]/h \qquad (7)$$

For example, in cyclohexane at $x = 4$ cm, $y = 6$ mm, $h = 0.20$ W/m·K, $\epsilon_b = 0.20$, $\epsilon_s = 1.0$. and Eq. (7) gives $T_g = 1600 + 56 - 0.09 - 0.03 - 0.06 = 1656$ K. Iteration is required since the gas conductivity is a function of the gas temperature, as given by Eq. (2). Initially, the gas temperature is taken to be the bead temperature for purposes of evaluating the conductivity; then, the approximate value of the gas temperature is used to re-evaluate the conductivity. Note that a similar procedure is not needed for the evaluation of the platinum emissivity, since this property is a function of the bead temperature, which is known.

An error analysis is carried out to determine the accuracy of the gas temperature correction. Since the major radiation term is due to emission from the bead, only this radiation term is used in the error analysis of the energy equation. The simplified balance gives the temperature correction

$$T_g - T_b = \Delta T = (\epsilon_b\sigma T_b^4)/h \qquad (8)$$

The fractional uncertainty in the temperature correction is

$$\frac{\sigma_{\Delta T}}{\Delta T} = \left[\left(\frac{\sigma_h}{h}\right)^2 + \left(\frac{\sigma_{\epsilon b}}{\epsilon_b}\right)^2 + 16\left(\frac{\sigma_{Tb}}{T_b}\right)^2\right]^{1/2} \qquad (9)$$

The accuracy of Eq. (1) for creeping flow should be within 10%, because of the spherical assumption, while the bead-diameter appears accurate to 3% and the uncertainty in k due to different species is assumed to be 3%. Therefore, h is ±10% accurate. The error in ϵ_b is small, < ±3% as shown in Fig. 3, except that ϵ_b is linear in T_b so error in T_b increases the uncertainty in ϵ_b. Outside the soot region, the voltage resolution of 1 μV yields a temperature accuracy of 0.1%. However, the position accuracy of ±0.1 mm also gives rise to an error in temperature measurement. In regions of maximum temperature gradient of ~500 K/mm, this placement error gives rise to a maximum error in bead temperature of ±50 K. Inside the soot region, extrapolating to zero time to eliminate the effects of soot buildup on the bead, gives an inaccuracy in T_b estimated at ±3%. Thus, the total estimated error in T_b is ±6% in the soot layer and 3% in the soot-free regions. Therefore, Eq. (9) suggests ΔT is accurate to ±30% in the soot layer and ±15% in the soot-free regions. Typical soot ΔT of 50 K are accurate to within ±15 K as are higher flame ΔT of 100K. Finally, the accuracy of T_g is given by

$$\frac{\sigma_{Tg}}{T_g} \approx \left[\left(\frac{\sigma_{Tb}}{T_b}\right)^2 + \left(\frac{\Delta T}{T_b}\right)^2\left(\frac{\sigma_{\Delta T}}{\Delta T}\right)^2\right]^{1/2} \qquad (10)$$

so that the accuracy of T_g is approximately that of T_b.

Velocity Field

A dual-beam differential laser Doppler velocimetry (LDV) system using the fringe mode is employed in this work. The 514.5 nm line of a 2 W argon-ion laser is split into two beams of equal intensity and then crossed to produce interference fringes in the probe volume. A seed particle passing across the light and dark fringes produces a scattering pattern that a photodetector picks up as a fluctuating signal proportional to the particle velocity.[22] First developed to measure velocities in cold flows,[23] use of LDV (also called LDA, laser Doppler anemometry) has grown to be a common tool for measuring flow velocities in many difficult flowfields including combustion.[24-28] Combusting flows offer an additional challenge to measurements using LDV since it is necessary to seed the flow with particles that follow the flow,[15] scatter the laser light, and do not burn up. A counter-type signal processor is used to measure the instantaneous velocity on a particle by particle

basis. The processor measures the time for a fixed number of Doppler cycles. This can be converted to the flow velocity by knowing the number of cycles measured and the interference fringe spacing in the probe volume. All of these particle velocities are stored as velocity histograms (see Fig. 4) in a minicomputer.

Velocity measurements are made at 0.5 mm increments in the horizontal or y direction and at two elevations, 2 and 4 cm, above the leading edge of the flame in the vertical or x direction. In the horizontal direction, the burner is positioned using a finely threaded rod with a digital micrometer accurate to 0.01 mm. The origin inaccuracy of $q \pm 0.1$ mm dominates the y direction accuracy. A typical velocity histogram is shown in Fig. 4a for iso-octane fuel at $y = 5$ mm from the fuel surface and $x = 4$ cm from the flame boundary-layer leading edge. The mean velocity of 86.86 cm/s is shown and the standard deviation from the mean (shown as turbulent intensity) is 4.7% for the 2000 data points taken. As seen by the sharp spike, most of the data falls near 87 cm/s. An example of a poor histogram taken at the same location is shown in Fig. 4b. The spread in velocity readings is most likely due to the flame flickering as the fuel supply is nearly exhausted. The mean velocity is not the same as for the better data seen in Fig. 4a and the turbulent intensity is higher (13.6%). Attempts were made to acquire data with the lowest possible turbulent intensity. The mean downstream velocities from these histograms are plotted vs horizontal position as in Fig. 5. The x component of the thermophoretic force is negligibly small.[13,15] The y component helps to send seed particles down the temperature gradient toward the wall across the converging streamline. These wicks were reduced to 5 cm wide so that the closest measurable point is 1 mm from the wick surface. Measurements closer to the wick were not possible due to blocking of the laser beams by the wall. The edge effects are confined to less than the boundary-layer thickness. As shown in Fig. 6, this is less than 1 cm at the x discussed above. Therefore, the inner 3 cm on the 5 cm wide block used in the velocity measurements and the inner 13 cm on the 15 cm wide block used in the temperature measurements are the same two dimensional flow. The wider block had been used to obtain sufficient attenuation in related soot studies.[1] The centerline fields are the same for both widths. Representative error bars are shown on various data points that indicate the standard deviation about the mean velocity measurement.

The signal was found to be very weak in the back scatter mode, so it was necessary to add a collimating lens and a corner cube to simulate a forward scatter system. This arrangement reflects the laser beams back on themselves so the particles scatter the reflected light in the same fashion as a forward scatter LDV system. This increased the signal strength by two orders of magnitude.

The seed particle generator is a fluidized-bed-type that seeds the flow with aluminum oxide particles having a mean diameter of 1 μm. The relatively low velocity of the flame

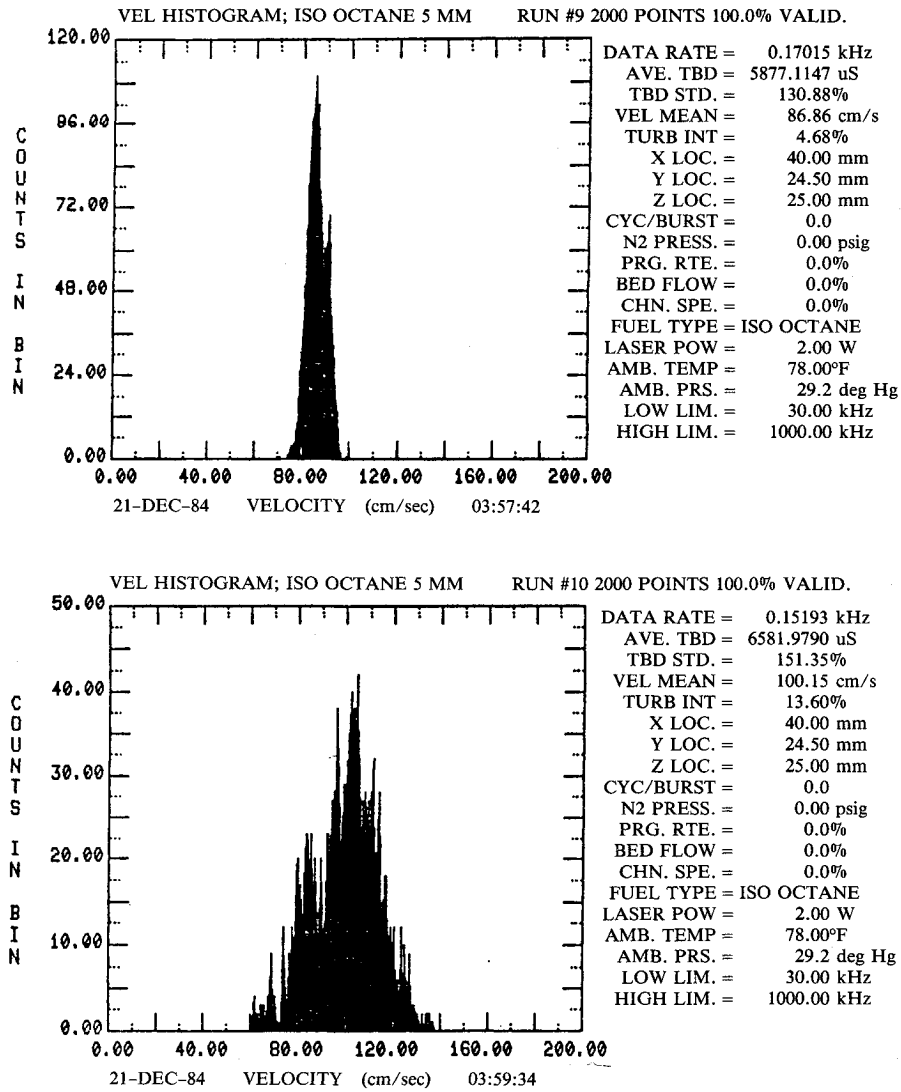

Fig. 4 Good and poor velocity histograms for iso-octane 2 cm downstream and 5 mm from the wall. The good data are from a steady, smooth flame and the poor data from a fluctuating flame as the wick begins to run dry.

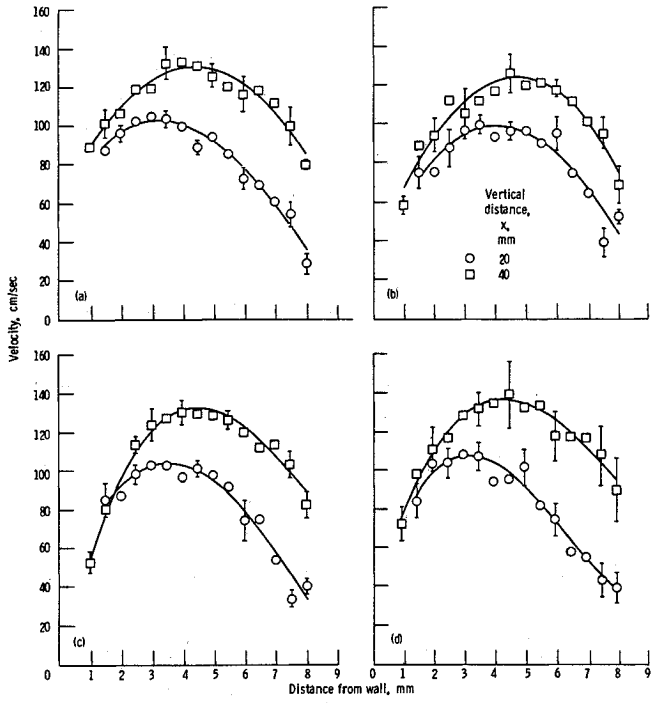

Fig. 5 Experimental velocity profiles at 2 and 4 cm downstream with experimental error bars of one standard deviation: a) n-heptane, b) cyclohexane, c) isooctane, and d) ethanol.

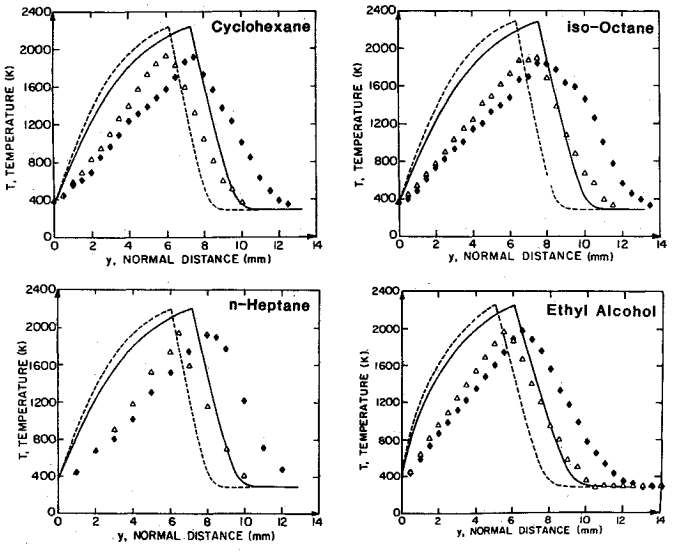

Fig. 6 Experimental and theoretical gas temperature profiles for cyclohexane, n-heptane, isooctane, and ethyl alcohol at 2 and 4 cm downstream. The accuracy of the measured temperatures is ±6% in the soot layer and ±3% elsewhere. The position accuracy in Figs. 5, 6, and 8 in within ±0.1 mm.

makes it difficult to find a seeding technique that does not interfere with the flow. Small, high-flow-velocity, fluidized-bed particle generators blew out the flame even with attempts to diffuse the seed flow. A large seed generator (450 l/min, 10–100 mg/m^3 mass output, 10^5 particle/cm^3) emerged as the best technique. The burner was surrounded by a Plexiglas enclosure with an exhaust hood. The exhaust fan is used after each run to clear the exhaust products and turned off prior to introducing the seed particles. The ceramic fiber board was soaked with liquid fuel until saturated, positioned in the marinite wall, and held in place with the marinite spacer. For the data taken at the $x=4$ cm position, the burner was ignited and the seed generator was then used to fill the enclosure with a cloud of aluminum oxide particles. The flame was allowed to stabilize until visibly smooth before taking data. At the $x=2$ cm position, the boundary layer was thinner and had less outside air entrainment, making it more difficult to seed. Therefore, it was necessary to fill the enclosure with seed particles first and then light the flame to insure that more particles were entrained into the flow.

Discussion

The analytical profiles of temperature and velocity which are presented in this paper are obtained from results reported by Beier et al.[2] This solution assumes unity Lewis number, transport properties independent of composition, constant $\rho\mu$, constant mixture specific heat, and fast flame kinetics and incorporates soot radiation using a uniform absorption coefficient. The problem of property evaluation, i.e., $\rho\mu$ and c_p, has been discussed.[2,3] The value of the soot absorption coefficient used in this analysis is obtained from the measured soot volume fractions.[1] Comparison of the temperature and velocity profiles predicted by this analytical solution with the experimental profiles reveals deficiencies in the determination of both profiles. As the emphasis of this report lies with the experimental measurements, a more detailed presentation of improvements in the analytical treatment will be deferred.[29]

The temperature measurements are corrected as in Eq. (7) and plotted as profiles across the boundary layer. Figure 6 shows corrected experimental measurements and theoretical predictions of temperature for cyclohexane, n-heptane, isooctane, and ethyl alcohol. These profiles reveal some common trends. The experimental profiles are almost linear from the wall to the flame layer, then fall off almost linearly to the ambient temperature. The theoretical temperatures are higher than the measured temperatures and bow up from the wall to the flame zone. They also fall off to ambient faster than the experimental temperatures, underpredicting temperatures in the outer regions of the flame. These deviations are due to several effects not included here, such as thermal cracking of the fuel and finite kinetics. The predictions include radiation; however, the model allows for soot emission as a global average which may spread out the energy sink effect of the soot emission over the boundary layer. Typical soot profiles are shown in Fig. 7 (from Ref. 1). An improved soot energy

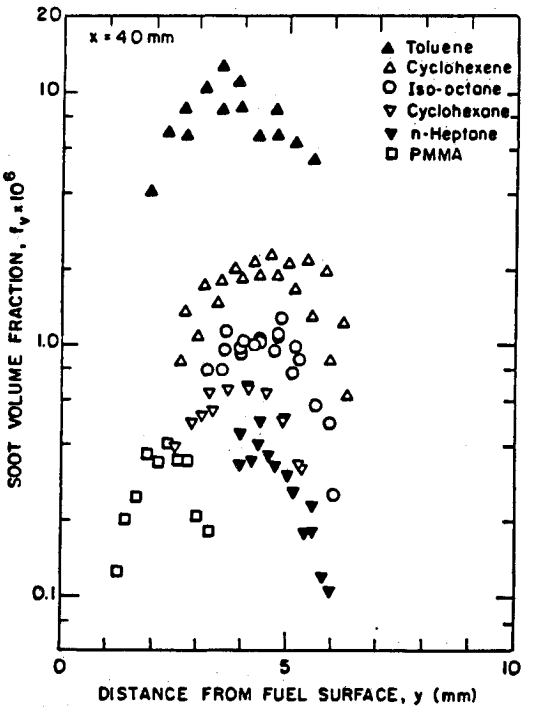

Fig. 7 Soot volume fractions f_v as a function of distance from the fuel surface, 4 cm downstream for isooctane, cyclohexane, n-heptane and other fuels from Ref. 1. Ethanol is below scale.

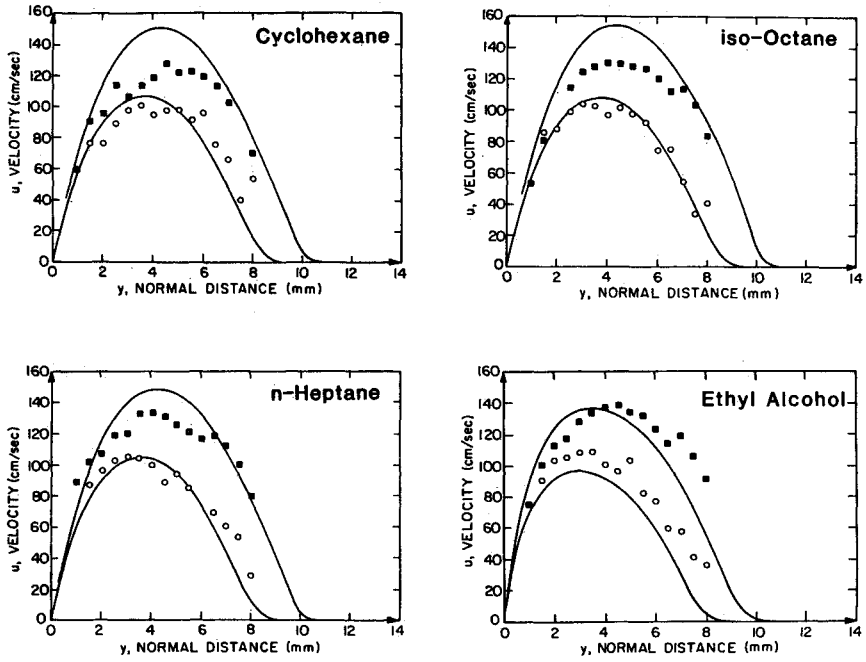

Fig. 8 Experimental and theoretical streamwise velocity profiles for cyclohexane, n-heptane, iso-octane, and ethyl alcohol at 2 and 4 cm downstream from the leading edge of the fuel wick.

sink model has been developed.[29] However, the essentially nonsooting ethyl alcohol flames also exhibit the same deviations, suggesting the endothermicity of the fuel pyrolysis[8] is responsible for the lower experimental temperatures between the wall and the flame.

The measured velocity profiles for cyclohexane, n-heptane, isooctane, and ethyl alcohol are compared with theory in Fig. 8. Included with these profiles are parabolic least squares curve fits to the experimental data. Agreement of velocity profiles with the theoretical predictions are quite good at the 2 cm location. The peak velocities of experimental and theoretical profiles are in good agreement. But a comparison of the curve fits with the theoretical curves reveals that the experimental data follow a broader profile. This is expected, since the experimental temperature profiles are broader than predicted. The 4 cm data show a stronger departure from the theoretical solution because the velocity profile is broader and lower than predicted. Some lowering of the peak may be expected since the peak temperature is over predicted. However, fluctuations should exert more influence downstream as the local Grashof number increases. Since this matches observations, fluctuations are the most probable cause of the measured velocity peaks being low.

Conclusions

The measurement of temperatures in flames is often accomplished by using thermocouples, sodium line reversal, the Kurlbaum technique, or various laser scattering methods. The least costly and most common method involves the use of thermocouples. In this study, the viability of using uncoated thermocouples with radiation corrections for diffusion flames is demonstrated. By incorporating the variation of gas conductivity and platinum emissivity with temperature in the energy balance of convection and radiation on the bead, accuracies on the order of 6% (soot) and 3% (no soot) appear achievable. A comparison of the experimental and theoretical results reveals that the analytical treatment of combusting boundary-layer flow needs refinement. However, the deviation between the experimental and analytical profiles cannot be completely attributed to soot emission. The similarity of the temperature profiles for these fuels with very different soot f_v concentrations suggests that another effect is causing the large deviation in temperatures. This has motivated a current study of thermal cracking of the fuel. Thermal cracking is an endothermic process in which the fuel decomposes into more stable smaller species. The results of this work will be presented in a forthcoming report.[30]

Acknowledgments

This work was supported by the Center for Fire Research of the National Bureau of Standards under Grant 60NANB5D0552. The velocity measurements were made at the NASA Lewis Research Center. The senior author also received support from a National Science Foundation Graduate Fellowship.

References

[1]Beier, R. A. and Pagni, P. J., "Soot Volume Fraction Profiles in a Free Combusting Boundary Layer," ASME Paper 81-HT-1, 1981.

[2]Beier, R. A., Pagni, P. J., and Okoh, C. I., "Soot and Radiation in Combusting Boundary Layers," *Combustion Science and Technology*, Vol. 39, 1984, pp. 235-262.

[3]Pagni, P. J. and Okoh, C. I., "Soot Generation within Radiating Diffusion Flames," *Twentieth Symposium (International) on Combustion*, The Combustion Institute, Pittsburgh, PA, 1984, pp. 1045-1054.

[4]Kim, J. S., de Ris, J., and Kroesser, F. W., "Laminar Free Convective Burning of a Surface," *Thirteenth Symposium (International) on Combustion*, The Combustion Institute, Pittsburgh, PA, 1971, pp. 949-961.

[5]Kosdon, F. J., Williams F. A., and Buman, C., "Combustion of Vertical Cellulosic Cylinders in Air," *Twelfth Symposium (International) on Combustion*, The Combustion Institute, Pittsburgh, PA, 1969, pp. 253-264.

[6]Pagni, P. J. and Shih, T. M., "Excess Pyrolyzate," *Sixteenth Symposium (International) on Combustion*, The Combustion Institute, Pittsburgh, PA, 1976, pp. 1329-1342.

[7]Santorto, R. J., Yeh, T. T., and Semerjian, H. G., "The Transport and Growth of Soot Particles in Laminar Diffusion Flames," *Twenty-Third National Heat Transfer Conference Proceedings*, Pub. HTD-45, ASME, New York, 1985, pp. 57-69.

[8]Nakagawa, Y., Nishiwaki, N., and Hirata, M., "Effect of Combustion on a Laminar Boundary Layer," *Thirteenth Symposium (International) on Combustion*, The Combustion Institute, Pittsburgh, PA, 1971, pp. 813-819.

[9]Hirano, T. and Kanno, Y., "Aerodynamic and Thermal Structures of the Laminar Boundary Layer Over a Flat Plate with a Diffu-

sion Flame," *Fourteenth Symposium (International) on Combustion*, The Combustion Institute, Pittsburgh, PA, 1973, pp. 391-398.

[10]Hirano, T. and Kinoshita, M., "Gas Velocity and Temperature Profiles of a Diffusion Flame Stabilized in the Stream Over Liquid Fuel," *Fifteenth Symposium (International) on Combustion*, The Combustion Institute, Pittsburgh, PA, 1974, pp. 379-387.

[11]Ramachandra, A. and Raghunandan, B. N., "An Analysis of a Boundary Layer Diffusion Flame Over a Porous Flat Plate in a Confined Flow," *Combustion Science and Technology,* Vol. 38, 1984, pp. 59-73.

[12]Quinn, T. J., *Temperature, Monographs in Physical Measurement,* Academic Press, New York, 1983.

[13]Farrow, R. L., Lucht, R. P., Flower, W. L., and Palmer, R. E., "Coherent Anti-Stokes Raman Spectroscopy Measurements of Temperature and Acetylene Spectra in a Sooting Diffusion Flame," *Twentieth Symposium (International) on Combustion*, The Combustion Institute, Pittsburgh, PA, 1984, pp. 1307-1312.

[14]Eisner, A. D. and Rosner, D. E., "Experimental Studies of Soot Particle Thermophoresis in Nonisothermal Combustion Gases Using Thermocouple Response Techniques," *Combustion and Flame,* Vol. 61, 1985, pp. 153-166.

[15]Talbot, L., "Thermophoresis - A Review," *AIAA Progress in Astronautics and Aeronautics: Rarefied Gas Dynamics,* Vol. 74, edited by S. S. Fisher, AIAA, New York, 1981, pp. 467-488.

[16]Pollock, D. D., "Thermocouples in High Temperature Reactive Atmospheres,' *Combustion Science and Technology,* Vol. 42, 1984, pp. 111-113.

[17]Madson, J. M. and Theby, E. A., "SiO_2 Coated Thermocouples," *Combustion Science and Technology,* Vol. 36, 1984, pp. 205-209.

[18]Smyth, K. C., Miller, J. H., Dorfman, R. C., Mallard, W. G., and Santoro, R. J., "Soot Inception in a Methane/Air Diffusion Flame as Characterized by Detailed Species Profiles," *Combustion and Flame,* Vol. 62, 1985, pp. 157-181.

[19]Jakob, M., *Heat Transfer,* Vol. 1, Wiley, New York, 1949.

[20]Hodgeman, C. D. (ed.), *Handbood of Chemistry and Physics,* 42nd ed., CRC Press, Cleveland, 1960.

[21]Gubareff, G. G., Janssen, J. E., and Torborg, R. H., *Thermal Radiation Properties Survey,* 2nd ed., Honeywell Research Center, Minneapolis-Honeywell Regulator Co., Minneapolis, 1960.

[22]Stevenson, W. H., "Principles of Laser Velocimetry," *AIAA Progress in Astronautics and Aeronautics: Experimental Diagnostis in Gas Phase Combustion Systems,* Vol. 53, edited by B. T. Zinn, AIAA, New York, 1976, pp. 307-336.

[23]Yeh, Y., and Cummins, H. Z., "Localized Fluid Flow Measurements with an He-Ne Laser Spectrometer," *Applied Physics Letters,* Vol. 4, May 15, 1964, p. 176.

[24]Rambach, G. D., Dibble, R. W., and Hollenbach, R. E., "Velocity and Temperature Measurements in Turbulent Diffusion Flames," Sandia National Laboratories, Livermore, CA, Rept. SAND-79-8775, 1979.

[25]Dandekar, K. V. and Gouldin, F. C., "Temperature and Velocity Measurement in Premixed Turbulent Flames," AIAA Paper 81-0179, 1981.

[26]Durst, F., Melling, A., and Whitelaw, J. H., "The Application of Optical Anemometry to Measurement in Combustion Systems," *Combustion and Flame,* Vol. 18, 1972, pp. 197-201.

[27]Ikioka, L. M., Brum, R. D., and Samuelson, G. S., "A Laser Anemometer Seeding Technique for Combustion Flows with Multiple Stream Injection," *Combustion and Flame,* Vol. 49, 1983, p. 155.

[28]Chigier, N. A., "Combustion Diagnostics by Laser Velocimetry," *AIAA Progress in Astronautics and Aeronautics: Experimental Diagnostics in Gas Phase Combustion Systems,* Vol. 53, AIAA, New York, 1976, pp. 337-356.

[29]Ang, J. A., "Perturbed Boundary Layer Diffusion Flames," Ph.D. Dissertation, Mechanical Engineering, University of California, Berkeley, 1986.

[30]Mataga, T.G., Ang, J. A. and Pagni, P. J., "A Two Sheet Model for Fuel Pyrolysis and Reaction," presented at the Eastern States Section/Combustion Institute, Fall Meeting, 1987.